Geophysical Journal International

Geophys. J. Int. (2014) **199,** 382–390 doi: 10.1093/gji/ggu210
GJI Seismology

Envelope of coda waves for a double couple source due to non-linear elasticity

Ignacia Calisto[1] and Klaus Bataille[2]

[1]*Department of Geophysics, University of Concepcion, Concepcion, Chile. E-mail: macalist@udec.cl*
[2]*Department of Earth Science, University of Concepcion, Concepcion, Chile*

Accepted 2014 May 30. Received 2014 May 16; in original form 2013 September 10

SUMMARY

Non-linear elasticity has recently been considered as a source of scattering, therefore contributing to the coda of seismic waves, in particular for the case of explosive sources. This idea is analysed further here, theoretically solving the expression for the envelope of coda waves generated by a point moment tensor in order to compare with earthquake data. For weak non-linearities, one can consider each point of the non-linear medium as a source of scattering within a homogeneous and linear medium, for which Green's functions can be used to compute the total displacement of scattered waves. These sources of scattering have specific radiation patterns depending on the incident and scattered *P* or *S* waves, respectively. In this approach, the coda envelope depends on three scalar parameters related to the specific non-linearity of the medium; however these parameters only change the scale of the coda envelope. The shape of the coda envelope is sensitive to both the source time function and the intrinsic attenuation. We compare simulations using this model with data from earthquakes in Taiwan, with a good fit.

Key words: Theoretical seismology; Wave scattering and diffraction; Wave propagation.

1 INTRODUCTION

The propagation of seismic waves throughout an idealized infinite, homogeneous and linearly elastic medium is free of scattering. However, the propagation of high-frequency waves throughout the Earth suffers significant scattering, spreading their energy in space and time and generating coda waves. Understanding the nature of seismic coda can help the imaging of real earth models, and therefore the physical properties within the Earth. So far, coda waves have been widely interpreted as due to scattering from a random distribution of inhomogeneities throughout the medium. Therefore, many properties of these inhomogeneities have been determined for a variety of regions worldwide, and for different periods of time. Spatial and temporal variations of statistical properties of inhomogeneities have been associated with changes in physical properties of the medium, including the presence of fluids, development of cracks, amongst other properties. The variation of some of these properties has been associated with the occurrence of earthquakes, thus, they might depend on the stage within the seismic cycle. If this is so, it has far reaching implications towards understanding the physics of earthquakes and other geophysical and geological processes.

Based on the fact that laboratory experiments show that the relationship between stress and strain, for rocks close to the rupture condition, is not linear (Scholz 1990; Van Den Abeele *et al.* 2000), it has recently been suggested by Bataille & Calisto (2008) that non-linear elasticity could be considered as a source of scattering. In this study, they presented a theoretical description of scattering due to a non-linear elastic medium. In their model, the medium is homogeneous, isotropic and elastically non-linear. The non-linearity is described by a strain energy which is a power of strain to the second and fourth powers. Other authors have used different expressions, such as Murnaghan (1951) and McCall (1994), amongst others, which have expanded the strain energy up to the third power. The precise dependence is something that can be tested when predictions are compared against seismological observations.

Evidence that non-linear elasticity contributes to the coda was presented by Calisto *et al.* (2010), analysing TIPTEQ data (Gross *et al.* 2008), where controlled chemical explosions were used as primary sources. They determined the value of a parameter p defined as $u_1/u_2 = (M_1/M_2)^p$, where u_1 and u_2 are the observed displacements and M_1 and M_2 are the respective moments at the same source–receiver distance, for the case of TIPTEQ data correspond to two explosions of different charge sizes. This parameter p represents the dependence of the strength of the scattered waves on the strength of the incident wave. For heterogeneities p should be 1; for a non-linear medium of second order in strain p should be 2; for a third order in strain p should be 3, and so on. For TIPTEQ data, the average value is $p = 2.5 \pm 0.9$, clearly suggesting that scattering is due to non-linearity. In this paper, we extend previous work, considering a double couple as the primary source, in order to compare the model prediction, computed in Bataille & Calisto (2008), with earthquake data. As an example, we use the

observed coda envelope for Taiwan earthquakes recorded at several stations, and compare with the predicted envelope considering Global CMT Project's seismic moment tensor (Dziewonski *et al.* 1981; Ekström *et al.* 2012).

2 THEORY

When seismic waves generated by an earthquake propagate through an isotropic homogeneous medium with a non-linear elasticity, they will be perturbed. This perturbation produces scattering, contributing to the seismic coda.

One way to describe non-linear elasticity is by considering the particular constitutive relationship suggested by Bataille & Calisto (2008) in which the energy density is given by

$$W(I_1, I_2, I_3) = \left(aI_1^2 + bI_2 + cI_1^4 + dI_2^2 + eI_1^2 I_2\right)/2, \tag{1}$$

where I_1, I_2 and I_3 are strain (ε_{ij}) invariants: $I_1 = Trace(\varepsilon_{ij})$, $I_2 = Trace(\varepsilon_{ij}\varepsilon_{ij})$ and $I_3 = Det(\varepsilon_{ij})$. The parameters a and b are Lamé constants and c, d and e are the non-linear parameters. Hooke's law is obtained when $a = \lambda/2$, $b = \mu$ and the non-linear parameters are equal to zero.

Starting with the equation of motion $\rho\ddot{u}_i = \partial_j \tau_{ij} + f_i$ we used the energy density expression described above, in order to obtain the respective elastodynamic equation:

$$\begin{aligned}\rho\ddot{u}_i - a\varepsilon_{pp,i} - b\varepsilon_{ij,j} = {} & f_i + 6c\varepsilon_{pp}\varepsilon_{qq}\varepsilon_{kk,i} + 2d\left\{\varepsilon_{pq}\varepsilon_{qp}\varepsilon_{ij,j} + 2\varepsilon_{pq}\varepsilon_{qp,j}\varepsilon_{ij}\right\} \\ & + e\left\{\varepsilon_{pq}\varepsilon_{qp}\varepsilon_{kk,i} + \varepsilon_{kk}\varepsilon_{ll}\varepsilon_{ij,j} + 2\varepsilon_{kk}\varepsilon_{pq,i}\varepsilon_{qp} + 2\varepsilon_{kk}\varepsilon_{ll,j}\varepsilon_{ij}\right\}.\end{aligned} \tag{2}$$

By using a perturbation approach to solve the corresponding equation of motion we obtained

$$\rho\ddot{u}_i^l - a\varepsilon_{pp,i}^l - b\varepsilon_{ij,j}^l = f_i$$

$$\rho\ddot{u}_i^{nl} - a\varepsilon_{pp,i}^{nl} - b\varepsilon_{ij,j}^{nl} = F_i^{nl}(\varepsilon^l) + O\left[(\varepsilon^l)^2\varepsilon^{nl}, \varepsilon^l(\varepsilon^{nl})^2, (\varepsilon^{nl})^3\right],$$

where the equivalent force which represents the source of scattering is

$$\begin{aligned}F_i^{nl} = {} & 6c\varepsilon_{pp}^l\varepsilon_{qq}^l\varepsilon_{kk,i}^l + 2d\left(\varepsilon_{kl}^l\varepsilon_{lk}^l\varepsilon_{ij,j}^l + 2\varepsilon_{kl}^l\varepsilon_{lk,j}^l\varepsilon_{ij}^l\right) \\ & + e\left(\varepsilon_{pq}^l\varepsilon_{qp}^l\varepsilon_{kk,i}^l + \varepsilon_{pp}^l\varepsilon_{kk}^l\varepsilon_{ij,j}^l + 2\varepsilon_{pp}^l\varepsilon_{lk}^l\varepsilon_{kl,i}^l + 2\varepsilon_{pp}^l\varepsilon_{ij}^l\varepsilon_{kk,j}^l\right)\end{aligned} \tag{3}$$

and ε_{ij}^l is the strain tensor of the incident wave. The incident wave is considered as the linear solution to the elastodynamic equation with the earthquake as a source.

To compare the theory with observations, we compute the contribution to scattered waves due to this effect by using the Green's function (G_{ij}) to determine the displacement solution (Aki & Richards 2002),

$$u_i(x,t) = \int\int G_{ij}(x,x',t,t')F_j^{nl}(x',t')\mathrm{d}x'\mathrm{d}t'.$$

This is valid only for the case of weak scattering, for strong scattering the superposition does not hold.

We represent the earthquake as an external force given by a point moment tensor $f_j = -\partial_i M_{ij}^*$, where $M_{ij}^*(x,t) = M_{ij}(t)\delta(x)$. For this case, the displacement in the far field is given by

$$u_i^l(x,t) = \frac{1}{4\pi\rho\alpha^3 r}\gamma_i\gamma_j\dot{M}_{jk}l\left(t - \frac{r}{\alpha}\right)\gamma_k + \frac{1}{4\pi\rho\beta^3 r}(\delta_{ij} - \gamma_i\gamma_j)\dot{M}_{jk}\left(t - \frac{r}{\beta}\right)\gamma_k, \tag{4}$$

where $\gamma_i = \frac{r_i}{r}$, α and β are the P- and S-wave velocities, respectively, and r is the distance from the point source.

Calling $M_{ij}^\alpha = M_{ij}(t - \frac{r}{\alpha})$, $M_{ij}^\beta = M_{ij}(t - \frac{r}{\beta})$, $\ddot{M}^{\alpha(\beta)} = \gamma_i\ddot{M}_{ij}^{\alpha(\beta)}\gamma_j$, $\dddot{M}^{\alpha(\beta)} = \gamma_i\dddot{M}_{ij}^{\alpha(\beta)}\gamma_j$, $\ddot{N}^\beta = \gamma_i\ddot{M}_{ij}^\beta\ddot{M}_{jk}^\beta\gamma_k$, $P^\beta = \gamma_i\ddot{M}_{ij}^\beta\dddot{M}_{jk}^\beta\gamma_k$, $C^\alpha = \frac{1}{4\pi\rho\alpha^4 r}$, $C^\beta = \frac{1}{4\pi\rho\beta^4 r}$, then

$$\begin{aligned}F_i^{(nl)} = {} & 6(c+d+e)\frac{(C^\alpha)^3}{\alpha}\gamma_i\left(\ddot{M}^\alpha\right)^2\dddot{M}^\alpha + (2d+e)\left[C^\beta\frac{(C^\alpha)^2}{2\beta}(\ddot{M}^\alpha)^2\left(\dddot{M}_{ij}^\beta\gamma_j - \gamma_i\dddot{M}^\beta\right) + C^\alpha\frac{(C^\beta)^2}{2\alpha}\gamma_i\dddot{M}^\alpha\left(\ddot{N}^\beta - (\ddot{M}^\beta)^2\right)\right] \\ & + d\frac{(C^\beta)^3}{4\beta}\left[\dddot{M}_{ij}^\beta\gamma_j\left(\ddot{N}^\beta - (\ddot{M}^\beta)^2\right) + 2\ddot{M}_{ij}^\beta\gamma_j(P^\beta - \ddot{M}^\beta\dddot{M}^\beta) + \gamma_i\left(3(\ddot{M}^\beta)^2\dddot{M}^\beta - 2\ddot{M}^\beta P^\beta - \dddot{M}^\beta\ddot{N}^\beta\right)\right] \\ & + e\left[C^\alpha\frac{(C^\beta)^2}{\beta}\gamma_i\ddot{M}^\alpha\left(P^\beta - \ddot{M}^\beta\dddot{M}^\beta\right) + C^\beta\frac{(C^\alpha)^2}{\alpha}\ddot{M}^\alpha\dddot{M}^\alpha\left(\ddot{M}_{ij}^\beta\gamma_j - \gamma_i\ddot{M}^\beta\right)\right].\end{aligned} \tag{5}$$

When the source duration of the earthquake is small, and can be approximated by $\delta(t)$, the time dependence of the equivalent force F^{nl} is non-zero for the arrivals of P and S waves, and zero for their cross terms. Therefore,

$$\begin{aligned} F_i^{(nl)}(t) &= 6(c+d+e)\frac{(C^\alpha)^3}{\alpha}\gamma_i\left(\ddot{M}^\alpha\right)^2\dddot{M}^\alpha + d\frac{(C^\beta)^3}{4\beta}\left[\dddot{M}_{ij}^\beta\gamma_j\left(\ddot{N}^\beta-(\ddot{M}^\beta)^2\right)+2\ddot{M}_{ij}^\beta\gamma_j(P^\beta-\ddot{M}^\beta\dddot{M}^\beta)\right.\\ &\quad\left.+\gamma_i\left(3(\ddot{M}^\beta)^2\dddot{M}^\beta-2\ddot{M}^\beta P^\beta-\dddot{M}^\beta\ddot{N}^\beta\right)\right]\\ &= F_i^{\alpha(nl)}\left(t-\frac{r}{\alpha}\right)+F_i^{\beta(nl)}\left(t-\frac{r}{\beta}\right), \end{aligned} \tag{6}$$

where

$$F_i^{\alpha(nl)}\left(t-\frac{r}{\alpha}\right) = 6(c+d+e)\frac{(C^\alpha)^3}{\alpha}\gamma_i\left(\ddot{M}^\alpha\right)^2\dddot{M}^\alpha \tag{7}$$

$$F_i^{\beta(nl)}\left(t-\frac{r}{\beta}\right) = d\frac{(C^\beta)^3}{4\beta}\left[\dddot{M}_{ij}^\beta\gamma_j\left(\ddot{N}^\beta-(\ddot{M}^\beta)^2\right)+2\ddot{M}_{ij}^\beta\gamma_j(P^\beta-\ddot{M}^\beta\dddot{M}^\beta)+\gamma_i\left(3(\ddot{M}^\beta)^2\dddot{M}^\beta-2\ddot{M}^\beta P^\beta-\dddot{M}^\beta\ddot{N}^\beta\right)\right] \tag{8}$$

represent the interaction of the non-linearity of the medium with the incoming P and S waves, respectively. One can notice that F^α and F^β are orthogonal forces, with F^α in the radial direction, and F^β in the tangential direction. This interaction produces scattering with a specific radiation pattern dependent on the geometry of the moment tensor M_{ij}.

To calculate and plot the radiation pattern for a particular seismic moment tensor, we use the values of the seismic tensor moment for three earthquakes that we have considered for the data analysis, which we will describe in more detail in the next section. The radiation patterns for the earthquakes used in the data analysis are shown in Fig. 1, where the left-hand column represents the P component of the equivalent force (arrows), whilst the right represents the radiation pattern produced by the S component (arrows) of the source of scattering. For all the plots in Fig. 1 the black lobes are the P-wave amplitude and the blue lobes, the S-wave amplitude. The seismic moment tensor for each earthquake, obtained from Global CMT Project (http://www.globalcmt.org/CMTsearch.html, last accessed May 2013), are:

$$\mathbf{M1} = \begin{pmatrix} 0.15 & 0.45 & -0.21 \\ 0.45 & -0.81 & -0.37 \\ -0.21 & -0.37 & 0.66 \end{pmatrix} \times 10^{17}\text{Nm} \quad \mathbf{M2} = \begin{pmatrix} 0.48 & 0.20 & -1.85 \\ 0.20 & -1.78 & 4.77 \\ -1.85 & 4.77 & 1.30 \end{pmatrix} \times 10^{18}\text{Nm}$$

$$\mathbf{M3} = \begin{pmatrix} -3.04 & 3.07 & 1.59 \\ 3.07 & -2.22 & 1.04 \\ 1.59 & 1.04 & 5.26 \end{pmatrix} \times 10^{17}\text{Nm}.$$

To calculate the radiation pattern we considered the angular part of the expression of the non-linear force.

3 MODEL AND DATA

3.1 Modelling scattered waves

Using the above theory to compute F^{nl} we numerically calculate the envelope of the scattered waves, which travel through a non-linear elastic medium, as (Aki & Richards 2002)

$$u_i^{nl}(x,t) = \int\int G_{ij}(x,x',t,t)F_j^{nl}(x',t')\mathrm{d}x'\mathrm{d}t', \tag{9}$$

where we consider this as an integral over the isochrones (the surface where the scattered waves arrive at the same time) and over time. G_{ij} is the Green's function for a homogeneous medium. The simplest temporal function that we can consider to describe the source is the Dirac delta. For large earthquakes, it is convenient to use a finite temporal function, with the duration of the source included, which, for simplicity, we choose to be the Gaussian function. The envelope of scattered waves is sensitive to different temporal functions, as shown in Fig. 2. The shape of the envelope changes with the source duration, which depends on the earthquake magnitude. To compute the Green's function we use the seismic velocities and the value of the attenuation factor Q from the earth model PREM (Dziewonski & Anderson 1981).

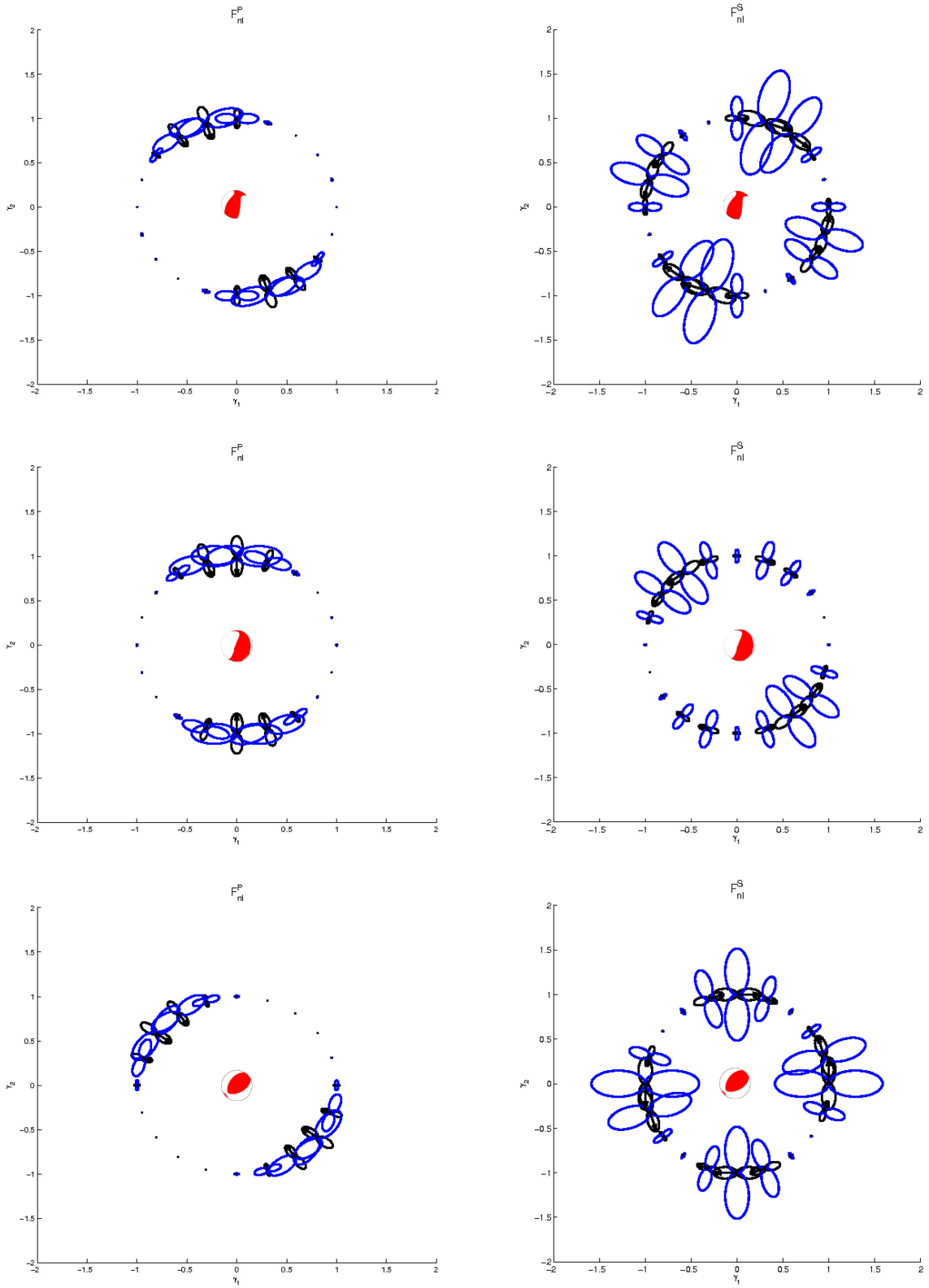

Figure 1. Radiation pattern of *P* waves (black lobes) and *S* waves (blue lobes) due to, on the left-hand column, the *P* component of the non-linear force (arrows) and, on the right-hand column, the *S* component of the non-linear force (arrows) for the three earthquakes that we are considering in this paper (see Table 1); each row indicates the earthquake under consideration (E_1, E_2 and E_3, respectively). The calculation was made considering a double couple source.

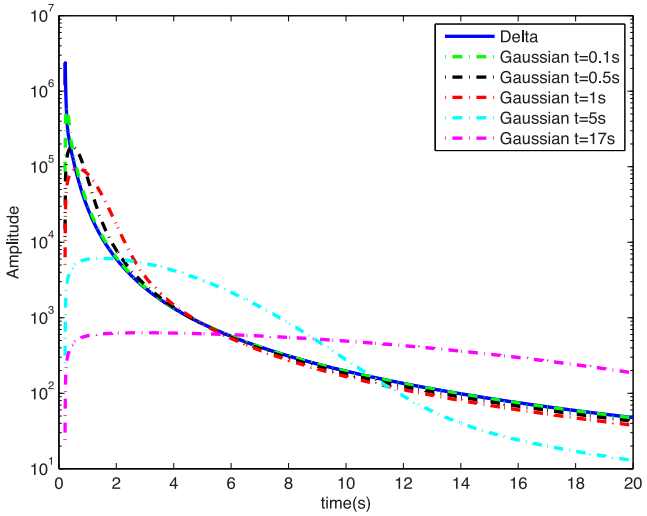

Figure 2. Envelopes of scattered waves using different temporal source time functions, such as Dirac delta and Gaussian functions for different source durations. The data used to perform the convolution between the observed data and temporal source is an explosion with a source–receiver distance of 1 km.

The resultant displacement calculated from eq. (9) is the sum of the interactions *PP*, *PS*, *SP* and *SS*, where

$$u_i^{PP} = \int G_{ij}^P F_j^\alpha = 6(c+d+e)\int G_{ij}^P \frac{(C^\alpha)^3}{\alpha}\gamma_j \left(\ddot{M}^\alpha\right)^2 \dddot{M}^\alpha$$

$$u_i^{PS} = \int G_{ij}^S F_j^\alpha = 6(c+d+e)\int G_{ij}^S \frac{(C^\alpha)^3}{\alpha}\gamma_j \left(\ddot{M}^\alpha\right)^2 \dddot{M}^\alpha$$

$$u_i^{SP} = \int G_{ij}^P F_j^\beta = d\int G_{ij}^P \frac{(C^\beta)^3}{4\beta}\left[\dddot{M}_{jk}^\beta\gamma_k\left(\ddot{N}^\beta - (\ddot{M}^\beta)^2\right) + 2\ddot{M}_{jk}^\beta\gamma_k(P^\beta - \ddot{M}^\beta\dddot{M}^\beta) + \gamma_j\left(3(\ddot{M}^\beta)^2\dddot{M}^\beta - 2\ddot{M}^\beta P^\beta - \dddot{M}^\beta\ddot{N}^\beta\right)\right]$$

$$u_i^{SS} = \int G_{ij}^S F_j^\beta = d\int G_{ij}^S \frac{(C^\beta)^3}{4\beta}\left[\dddot{M}_{jk}^\beta\gamma_k\left(\ddot{N}^\beta - (\ddot{M}^\beta)^2\right) + 2\ddot{M}_{jk}^\beta\gamma_k(P^\beta - \ddot{M}^\beta\dddot{M}^\beta) + \gamma_j\left(3(\ddot{M}^\beta)^2\dddot{M}^\beta - 2\ddot{M}^\beta P^\beta - \dddot{M}^\beta\ddot{N}^\beta\right)\right].$$

We see that each of these displacements is the product of the amplitude of the interaction and the shape given by the angular part of the non-linear force. The amplitude depends on the non-linear coefficients c, d and e. In order to estimate these parameters, firstly we 'normalize' by dividing each interaction by a normalization constant. In this case we use the amplitude of the interaction *PP* as the normalization constant; with this we obtain expressions which depend on $\frac{d}{(c+d+e)}$. This means that we do not need to know the exact values of the non-linear coefficients, only their relative values. To estimate the non-linear coefficients we will use the fact that they represent the perturbation of Hooke's law. By using the expression

$$\tau_{ij} = \left[aI_1 + 2cI_1^3 + eI_1I_2\right]\delta_{ij} + \left[b + 2dI_2 + eI_1^2\right]\varepsilon_{ij}$$

derived from eq. (1), where the values a and b are the Lamé parameters, we obtain the following comparisons:

(i) $2cI_1^3 \ll aI_1 \Rightarrow c \ll \frac{a}{2I_1^2} \sim 5\times10^{17}$
(ii) $eI_1I_2 \ll aI_1 \Rightarrow e \ll \frac{a}{I_2} \sim 1\times10^{18}$
(iii) $2dI_2 \ll b \Rightarrow d \ll \frac{b}{2I_2} \sim 5\times10^{17}$

which give us an idea about the non-linear coefficients (an upper limit). In the above equation we have used the value of ε to be approximately 10^{-4}. Despite the above inequalities showing that the non-linear coefficients have to be much less that the stated values, we can assume that they are very similar in orders of magnitude. Fig. 3 shows what happens with the model when we consider different values of $\frac{d}{(c+d+e)}$ by using different values of the non-linear constants. We used the following cases:

(i) $e = 5d = 10c \Rightarrow \frac{d}{c+d+e} = \frac{2}{13}$.
(ii) $e = 3d = 3c \Rightarrow \frac{d}{c+d+e} = \frac{1}{5}$.
(iii) $e = 2d = 2c \Rightarrow \frac{d}{c+d+e} = \frac{1}{4}$.
(iv) $e = 2d = 3c \Rightarrow \frac{d}{c+d+e} = \frac{3}{11}$.

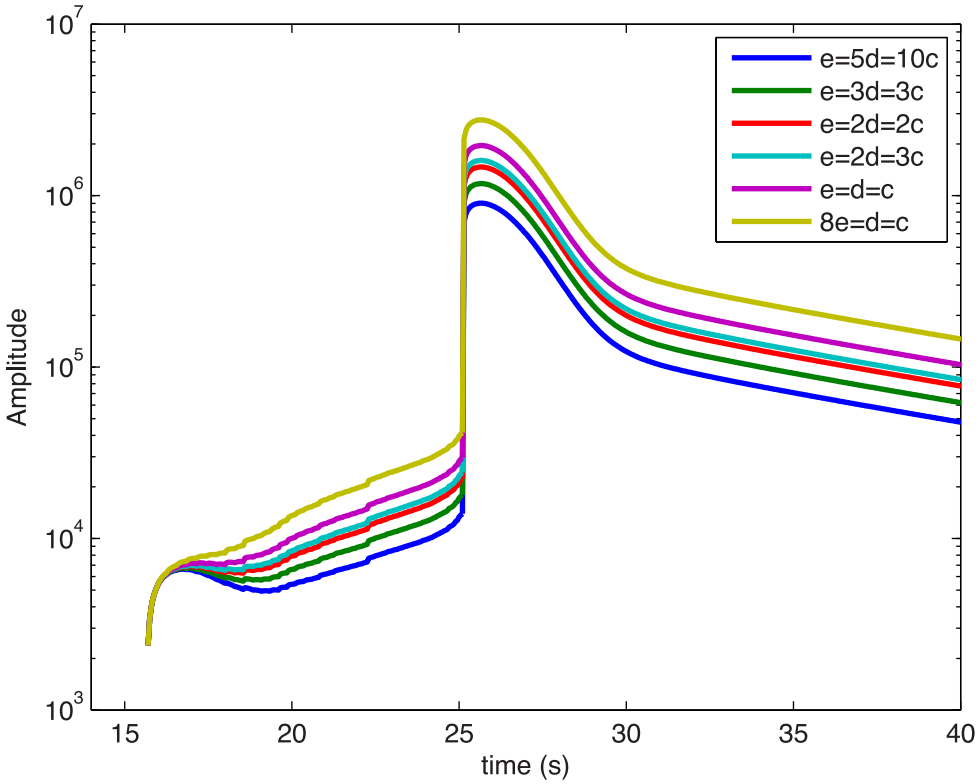

Figure 3. Comparison of model data using different combination of non-linear coefficients.

Table 1. List of earthquakes.

ID	Date		Lat	Lon	Depth (km)	M_w	Half duration (s)
E1	2010/04/11	04: 57	23.26	122.06	16.7	5.3	1.0
E2	2000/06/10	18: 23	23.84	121.23	15.0	6.4	4.3
E3	2000/09/10	08: 54	24.01	121.53	34.8	5.8	2.0

(v) $e = d = c \Rightarrow \frac{d}{c+d+e} = \frac{1}{3}$.
(vi) $8e = d = c \Rightarrow \frac{d}{c+d+e} = \frac{8}{17}$.

We see that the jump between the *P* and the *S* arrival depends slightly on the ratio between the non-linear coefficients, but not enough to have an appreciable difference in the total shape of the curve. From the *S* arrival to the end of the envelope, there is no shape change, only the amplitude is affected. Considering this, for simplicity we will use an intermediate case of $e = 2d = 2c$.

3.2 Data

The data that we use to compare observations with the model of non-linearity was obtained from different earthquakes in the Taiwan region, which are detailed in Table 1. The earthquake parameters, geometry and size, were taken from Global CMT Project and IRIS (http://www.iris.edu, last accessed May 2013). The data set was recorded with broadband seismometers, which are part of the Broadband Array in Taiwan for Seismology. Three seismograms and their envelopes, filtered between 5 and 10 Hz, at source–receiver distances between 39 and 147 km are shown in Fig. 4. The envelopes are smoothed to show the differences between them. The records are shifted in time, beginning at the observed arrival time of the *P* wave.

4 RESULTS

For the analysis we take the followings steps: (i) we filter the data with a bandpass filter between 5 and 10 Hz; (ii) we calculate the observed envelope of the vertical component seismograms; (iii) we calculate the synthetic envelope considering the non-linear elasticity, produced by the geometry of the source; (iv) we calculate the convolution between the isochron surface and the temporal function, which depends on the duration of the source and (v) we scale the numerical model to the observed data. Fig. 5 shows the fit between the model and observed data for the earthquakes E1, E2 and E3 (columns), which are recorded at stations NACB, TPUB and YULB (rows), with respective source–receiver distances of 112 km for E1-NACB, 147 km for E1-TPUB, 80 km for E1-YULB, 53 km for E2-NACB, 87 km for E2-TPUB,

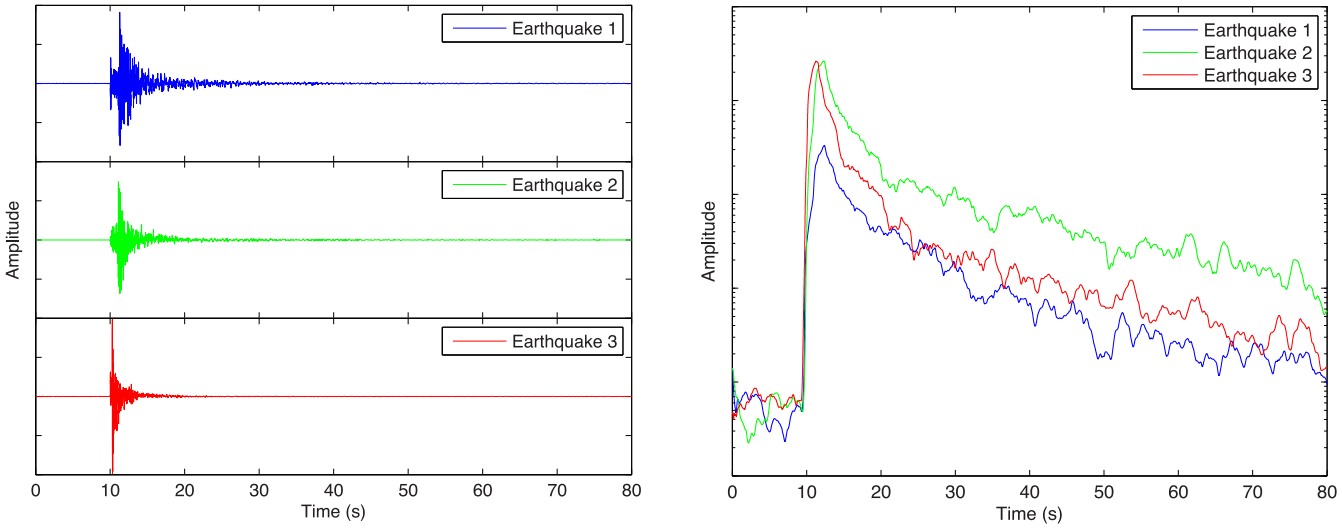

Figure 4. Seismograms (left-hand panel) and their smoothed envelopes (right-hand panel) of the earthquakes in the study. The envelope was computed using the program SAC. The method of smoothing used here is the moving average method with a 300 points used to compute the average. The source–receiver distance of the earthquakes varies from 39 to 147 km. The records are shifted in time, beginning at the observed arrival time.

52 km for E2-YULB, 39 km for E3-NACB, 125 km for E3-TPUB and 80 km for E3-YULB. The fit is good in all cases. These examples are representative of the average fit for approximately 50 seismograms for which we tested the model, which have different source–receiver distances and earthquake magnitudes.

5 DISCUSSION AND CONCLUSIONS

The non-linearity in the constitutive law has been shown to explain the coda of seismic waves due to an explosive source (Calisto *et al.* 2010). In the case when the source is modelled as a double couple, the fit between the modelled and the observed data is good. It is necessary to discriminate between non-linear elasticity and other sources of scattering; this paper is a first step in this direction.

The coda of seismic waves is due to scattering throughout the Earth. This scattering is thought to be due to the heterogeneities, but it may not be the only cause. We suggest that the non-linearity of the elastic medium should be considered. The main difference between these two sources of scattering is in the dependence of the amplitude of the incident wave. For a non-linear process, the strength of the scattered field is proportional to the amplitude of the incoming wave up to the third power (when the strain energy depends up to fourth order in the strain tensor), whilst for a heterogeneous medium, it is proportional to the first power. Therefore for small amplitudes or large distances the non-linear effect diminishes.

As for the energy partition of *S*- and *P*- waves in the coda, we calculated the quotient of the square amplitude of *P*- to *S*- and *S*- to *P*- converted waves obtaining a ratio which depends on the non-linear parameters and seismic velocities. Specifically, for the case of $e = 2c = 2d$ the ratio is close to 10 which is similar to the value obtained from heterogeneities (Ryzhik *et al.* 1996; Weaver 1982).

A rather powerful tool being used recently is the use of the cross-correlation between two stations to obtain the Green's function (Snieder 2004). For the case where the medium is weakly non-linear, we expect the cross-correlation represents the Green's function, but for strong non-linearity, the Green's function is less meaningful.

The shape of the calculated seismogram envelope depends weakly on the relative values of the parameters c, d and e, as is shown in Fig. 3. There is even a trade-off between variations of c, d and e keeping the sum $c + d + e =$ constant. The important point in this paper is to show that the shape of the envelope is completely modelled with the concept of a non-linear, instead of a heterogeneous medium. On the other hand, the amplitude could be fully estimated by calculating the non-linear parameters. We gave an upper limit for these parameters, however the exact calculation is not possible to perform because the observations contain information from different sources of scattering. For future work, we suggest the need to determine the absolute values of these parameters c, d and e, which will describe in more detail the origin of the non-linearity. A way to do this is to separate the scattering due the heterogeneities from non-linearity assuming that these two are the main sources of scattering, and then obtain the non-linear parameters of the medium.

The main point of this paper, is to show that the shape of the envelope of recorded seismograms, which originated from typical earthquakes, can be explained by scattering due to non-linear elasticity. This indeed we show in Fig. 5.

This non-linear theory is applicable as long as the non-linear elastic parameters are non-zero. A threshold, above which the non-linear theory can provide observable results, can be contemplated as the point where the product of the nonlinear term (consider c for instance), times the strain (ε) squared, is a fraction (10^{-2}) of the rigidity of the media. This fraction can be argued by taking the constitutive law of the stress being $\tau = \lambda I_1^2 + cI_1^4 + \ldots$ or $\tau = \lambda I_1^2(1 + \frac{c}{\lambda} I_1^2) + \ldots$. For the non-linear term to be significant, say to a threshold of 1 per cent, the value of I_1^2 should be approximately $10^{-2}\frac{\lambda}{c}$. This depends on the non-linear parameter c.

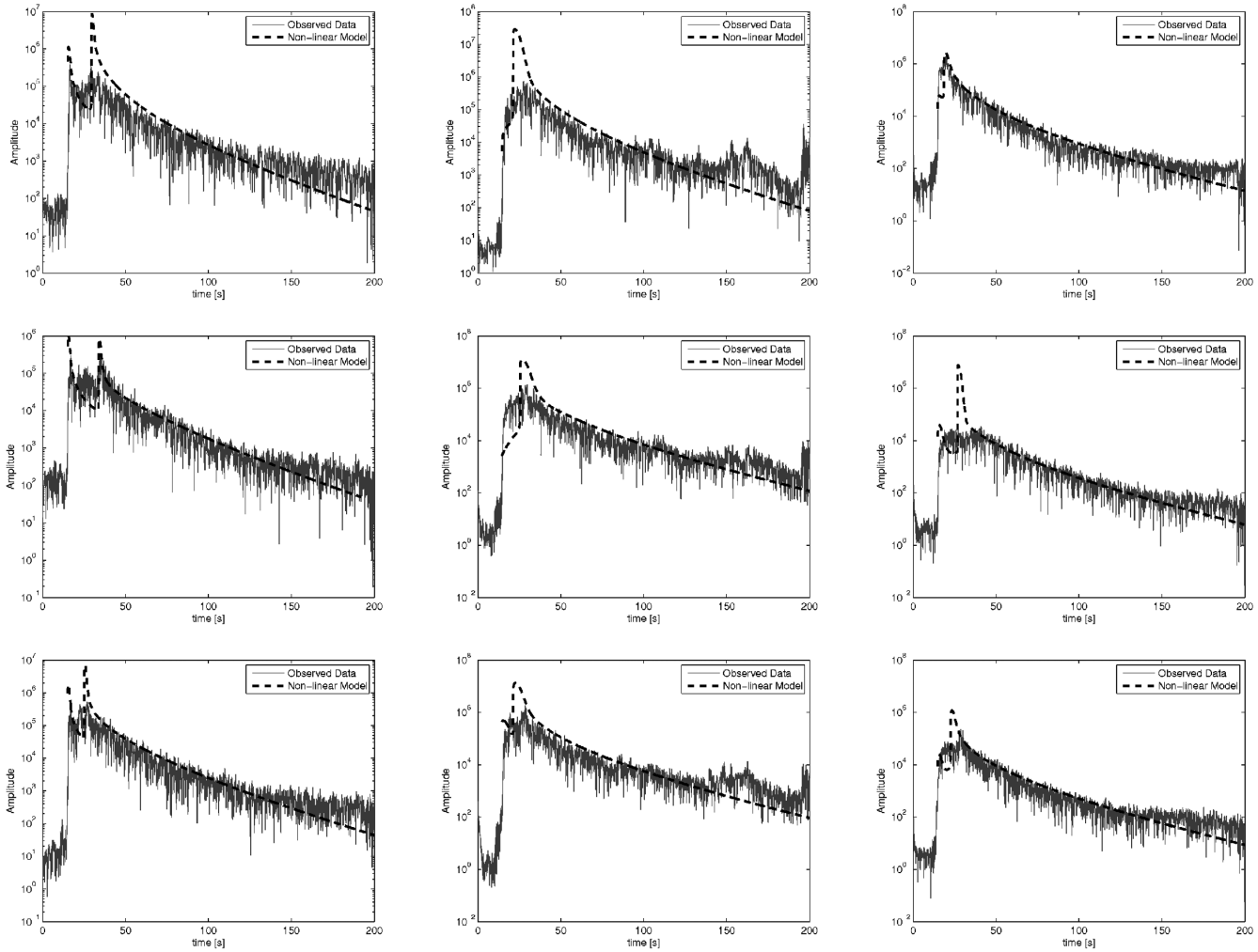

Figure 5. Model results compared with the envelopes of the earthquakes. Rows are the stations NACB, TPUB and YULB, columns are earthquakes E1, E2 and E3.

We have shown theoretically, and from earthquake data, that the scattering due to a non-linear elastic medium for a double couple source can contribute to the seismic coda. Further work is required to discriminate between scattering due to heterogeneities and due to non-linearity of the elastic medium and obtain the non-linear parameters in order to fully describe the scattering due to non-linear medium.

ACKNOWLEDGEMENTS

Thanks to the Broadband Array in Taiwan for Seismology for making their data public. Funding was provided by FONDECYT 3100095 (Calisto) and FONDECYT 1100990 (Bataille).

REFERENCES

Aki, K. & Richards, P.G., 2002. *Quantitative Seismology,* 2nd edn, University Science Books, 700 pp.

Bataille, K. & Calisto, I., 2008. Seismic coda due to non-linear elasticity, *Geophys. J. Int.,* **172**(2), 572–580.

Calisto, I., Bataille, K., Stiller, M. & Mechie, J., 2010. Evidence that non-linear elasticity contributes to the seismic coda, *Geophys. J. Int.,* **180,** 1353–1358.

Dziewonski, A. & Anderson, L., 1981. Preliminary reference Earth model, *Phys. Earth planet. Inter.,* **25,** 297–356.

Dziewonski, A., Chou, T. & Woodhouse, J., 1981. Determination of earthquake source parameters from waveform data for studies of global and regional seismicity, *J. geophys. Res.,* **86,** 2825–2852.

Ekström, G., Nettles, M. & Dziewonski, A., 2012. The global CMT project 2004–2010: Centroid-moment tensors for 13,017 earthquakes, *Phys. Earth planet. Inter.,* **200–201,** 1–9.

Gross, K. & Micksch, U. TIPTEQ Research Group Seismics Team, 2008. The reflection seismic survey of project TIPTEQ the inventory of the Chilean subduction zone at 38.2°S, *Geophys. J. Int.,* **172,** 565–571.

Lyakhovsky, V.A. & Myasnikov, V.P., 1988. Acoustics of rheologically non-linear solids, *Phys. Earth planet Inter.,* **50,** 60–64.

McCall, K.R., 1994. Theoretical study of non-linear elastic propagation, *J. geophys. Res.,* **99,** 2591–2600.

Murnaghan, F.D., 1951. *Finite Deformation of an Elastic Solid,* 1st edn, John Wiley and Sons, Inc.

Ryzhik, L.V., Papanicolau, D.C. & Keller, J.B., 1996. Transport equations for elastic and other waves in random media, *Wave Motion,* **24,** 327–370.

Scholz, C.H., 1990, *The Mechanics of Earthquakes and Faulting,* Cambridge Univ. Press, 439 pp.

Snieder, R., 2004. Extracting the Green's function from the correlation of coda waves: a derivation based on stationary phase, *Phys. Rev. E,* **69,** 046610.

Van Den Abeele, K.E.-A., Johnson, P.A. & Sutin, A., 2000. Nonlinear elastic wave spectroscopy (NEWS) techniques to discern material damage. Part I: nonlinear wave modulation spectroscopy (NWMS), *Res. Nondestr. Eval.,* **12,** 17–30.

Weaver, R.L., 1982. On diffuse waves in solid media, *J. acoust. Soc. Am.,* **71,** 1608–1609.